Cryogenics 127 (2022) 103564

Contents lists available at ScienceDirect

Cryogenics

journal homepage: www.elsevier.com/locate/cryogenics

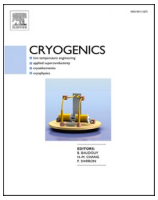

Experimental and numerical investigation of open-cycle miniature Joule-Thomson cryocooler for working temperatures 100 K to 150 K with single component coolants

Alexander Shapiro [a,*], Mordechai Greenberg [a], Anatoly Parahovnik [b]

[a] Cryogenics group RAFAEL, Haifa, Israel
[b] University of Central Florida, Orlando, USA

ARTICLE INFO

Keywords:
Joule-Thomson cryocoolers
Open cycle
Cooling materials
Heat transfer

ABSTRACT

Krypton and R14 (i.e. single component gasses) were studied as potential coolants for an open cycle miniature Joule-Thomson cryocooler. Cooling experiments were performed at ambient temperatures of 293 K and 343 K followed by theoretical analysis and parameter decomposition. The theoretical analysis identified the isothermal effect, heat exchanger efficiency, and the mass flow rate as the governing parameters for cooling performance. A detailed analysis indicated that the effective cooling power of the cryocooler was influenced mostly by the mass flow rate. As a result, krypton had a Cool Down Time shorter by 27% and Cooling Duration Period longer by 8%, compared to R14.

1. Introduction

Joule-Thomson (JT) cryocoolers are widely used in various applications where attaining cryogenic temperatures is needed. Among these applications can be found cryosurgery and the liquefaction of natural gas. Additional relatively common use is the cooling of infrared detectors in missile guidance systems, which are cooled to characteristic temperatures of liquid nitrogen, (i.e. approximately 80 K) [1]. Generally, a Joule-Thomson cryocooler can work either in open or closed cycle. However, the compressor, required for a closed cycle configuration adds complexity and reduces the reliability of the cooling system. Therefore, open cycle is preferred for applications where high reliability is required. Additionally, due to the higher initial pressure of an open loop vessel compared to a common closed loop compressor discharge, open loop cycles usually provide faster cooldown times that are essential in certain applications.

IR vision High Operating Temperature (HOT) detectors are a new type of devices with reduced cooling heat load due to higher operational temperatures (i.e., about 150 K). For these elevated temperatures, the cooldown time become shorter, and the cooling duration can be prolonged for a given vessel. Consequently, HOT detector enables to design open loop cryocooled IR vision systems with better performances for the same amount of coolant. Recent advances in developing of HOT detectors that require a working temperature range of 130 K to 175 K [2] makes them a viable solution.

In the present research it was decided to consider working temperatures of 100 K to 150 K.

Radebaugh et al. [3] presented a concept of a five-stage cascade cryocooler with R14 as the main coolant for achieving cooling temperature of 145 K. The study demonstrated the feasibility of R14 as a coolant because of its boiling temperature of 145 K at normal pressure (i.e. 1 atm). Piotrowska et al. [4] researched a five-component mixture, a mix of nitrogen and different hydrocarbons, which was utilized in a single-stage cryocooler. The work showed a stable 4 W to 12 W cooling capacity at working temperatures of 90 K to 120 K. The repeatability of the mixture was tested over 28 days of continuous cooling and a 5 K to 7 K shift at the working temperature was measured. The last result led to the conclusion of uncertain repeatability of the investigated mixture. Tzabar [5] researched nitrogen-ethane mixtures with molar ratios of 0.4/0.6, 0.55/0.45, 0.7/0.3 and nitrogen-propane mixtures with molar ratio of 0.6/0.4. Tzabar calculated the isothermal effects (Δh_T) of the mixtures and verified it with complementary experiments. Tzabar concluded that a nitrogen-ethane mixture with more than 55% of nitrogen showed promising performance for cooling to temperatures above 100 K. Walimbe et al. [6] presented an experimental result of cooling with non-flammable mixtures of four and five components for cold temperatures around 125 K. However, the cooling temperatures were not stable and depended on the heat load. Xu et.al [7–8] developed a method for calculating the thermodynamic properties, the boiling and

* Corresponding author.
E-mail address: alexsha@rafael.co.il (A. Shapiro).

https://doi.org/10.1016/j.cryogenics.2022.103564
Received 30 June 2021; Received in revised form 12 August 2022; Accepted 4 September 2022
Available online 8 September 2022

Nomenclature

A	Area m^2
C	Heat capacity, $J \bullet s^{-1} \bullet K^{-1}$
c_p	Specific heat capacity, $J \bullet kg^{-1} \bullet K^{-1}$
D, d, d_t	Diameter, m
D_H	Hydraulic diameter, m
E,Er_r	Error
H	Enthalpy, J
h	Specific enthalpy, J/g
HTC	Convection heat transfer coefficient $W \bullet m^{-2} \bullet K^{-1}$
Δh_T	Isothermal effect, J/g
i	Index
k, k_t	Thermal conductivity, $W \bullet m^{-1} \bullet K^{-1}$
L	Length, mm
$\dot{m}$	Flow rate, g/s
P	Pressure, MPa
$\dot{P}$	Pressure rate MPa/s
Pr	Prandtl number
Re	Reynolds number
$\dot{Q}$,	Heat load, W
$\dot{Q}_{eff}$	Effective cooling power, W
q	Heat transfer rate, W
T	Temperature, K
T_{amb}	Ambient temperature, K
U	Overall heat transfer coefficient
V	Volume m^3

Greek symbols

Δ	Difference between two states
ε	Heat exchanger effectiveness
η	Effiency
η_{fin}	Fin efficiency
μ	Dynamic viscosity, Pa•s
ρ	Gas density $g \bullet m^{-3}$
$\dot{\rho}$	Gas density rate, $g \bullet m^{-3} \bullet s^{-1}$

Abbreviations and acronyms

CDT	Cool down time
CDP	Cooling duration period
CFHE	Counter Flow Heat Exchanger
CP	Cut off pressure
EDM	Electrical Discharge Machining
HOT	High Operating Temperature
JT	Joule-Thomson
min	Minimal
NTU	Number of transfer units
TS	Temperature sensor

subscripts

Ng	Data taken from Ng. et al. paper [16]
Cur.Sim	Current simulation

the freezing temperatures of the binary flammable and non-flammable mixtures. The flammable mixtures contained nitrogen with different hydrocarbons, and the non-flammable mixtures contained nitrogen with freon. The phase diagram of different mixtures was verified with experimental data. It was concluded that the considered mixtures were viable as coolants. Geng et al. [9] performed an extensive review and surveyed various works on closed cycle JT cooling with many investigated mixtures and eventually provided a range of 65 K to 200 K of working temperatures. Shapiro et al. [10], analytically checked the feasibility of a binary mixture containing krypton and R14 for cooling below 150 K. The research goal was to achieve stable working temperature below 145 K at low pressure up to 0.24 MPa. A mixture of krypton and R14 with a molar ratio of 0.75/0.25 was identified as the most promising option.

A common configuration of a miniature JT cryocooler employs a Hampson-type recuperative, counter-flow heat exchanger. This configuration utilizes a finned tube that is coiled on a mandrel and was encapsulated in a concentric tube. In this setup, the high-pressure and high-temperature coolant flow within the tube, and the low-pressure and low-temperature coolant (i.e., the coolant after throttling) flows towards the outlet between the mandrel the concentric tube [11]. The heat exchanger is a vital component responsible for cryocooler's performance and, therefore, needs to be carefully analyzed. Partitioning the heat exchanger into subsections and solving the mass, momentum, and energy equations for each subsection is a common technique that is widely implemented in research of Hampson-type heat exchangers [12–18]. Ardhapurkar and Atrey [11], and Damle and Atry [12] theoretically studied the Hampson-type heat exchanger with nitrogen and argon as working coolants, for steady state and transient analysis. These works compared the numerical results with the experimental data available in the literature, and concluded that an area correction coefficient is a sufficient corrective parameter to predict the experimental results. Gupta et al. [13,14], experimentally researched the Hampson-type heat exchanger for pressure drop and heat transfer characteristics using helium as a coolant. This work predicted the pressure drop and convective heat transfer coefficient within 5%, and 10% accuracy, respectively. Mehta et al. [15], employed the technique to optimize heat exchangers in a helium liquification plant. The optimized configurations were later tested and yielded a good fit with the theoretical model. Ng et al. [16], studied both experimentally and numerically the performance of Hampson-type heat exchanger with argon as a coolant. This work accounted for radial and axial losses and resulted in a 3% accuracy compared to the pertinent experimental results. Tzabar [17] theoretically studied the performance of Hampson-type heat exchangers and verified the developed analysis with experimental data. Tzabar [17] used the model to outline the governing parameters and to optimize the geometrical characteristics of the cryocooler's heat exchanger. It is a valid conclusion that the subdivision of Hampson-type heat exchanger is a suitable method to explore the thermal performances of the heat exchangers that are a cardinal component in JT cryocoolers.

The pure inert gases have advantages as a potential coolant. They are non-flammable, easy to simulate, and lacking a pinch point [5,10]. Therefore, a single-component gas is a favorable coolant and justifies further research. Currently, single component coolants (i.e., typically nitrogen, argon, and air) mostly accommodate cooled detector with working temperatures about 80 K. For HOT detectors, most of the published works discuss multi-component coolants and closed-cycle JT cryocooling configurations. To the best of our knowledge, the available experimental data about single-component, open-cycle JT cryocooling for 100 K to 150 K working temperature range is scarce. Therefore, the purpose of this present work is to discuss pure gases as candidates for open-cycle JT cooling for working temperatures of 100 K to 150 K. After reviewing boiling and freezing temperatures of several coolants, it was decided to concentrate on krypton and R14. Thermodynamic and heat transfer properties, such as the isothermal effect and the NTU of the heat exchanger were calculated and compared. Finally, an experimental setup was assembled, and open-cycle cooling tests were performed at 293 K and 343 K ambient temperatures.

In this paper the theoretical treatment was restricted to that of the recuperative heat exchanger on account of its relatively low complexity

Table 1
Potential coolants list.

Coolant name	Chemical formula	Boiling temperature [K]	Freezing temperature [K]
Isobutane	C_4H_{10}	261.4	113.7
Hexafluoroethane / R116	C_2F_6	195.1	173.1
Chlorotrifluoromethane / R13	C_1F_3	191.7	92
Trifluoromethane / R20	CHF_3	191.1	118
Ethane	C_2H_6	184.6	90.4
Ethylene	CH_2	169.4	104
Tetrafluoromethane / R14	CF_4	145.1	89.5
Krypton	Kr	119.7	115.8
Methane	CH_4	111.7	90.7

and, on the other hand, fundamental role in the cryocooler performance. Heat exchange's analysis was sufficient to compare the coolants and to highlight the differences in their performances.

1.1. Theoretical study

The following section outlines and compares the potential coolants, then discusses the cooling capacity using the isothermal effect of the best two candidates, and finally presents the theoretical model that was used to analyze the experimental results.

1.2. Potential coolants

Various pure coolants were listed with their boiling and freezing temperatures at normal conditions, using REFPROP^{TM} [19]. The potential coolants then were sorted according to their boiling temperature, isobutane and methane had the highest and lowest boiling temperatures of 261.4 K and 111.7 K, respectively (Table 1). For the desired range (i.e., from 100 K to 150 K) the potential coolants were R14, krypton, and methane. R14 is a refrigerant that is widely used in the microelectronic industry, and when combined with oxygen it forms a plasma etchant for silicon [20]. Methane is a hydrocarbon, and among other application is widely used as a component in rocket fuel [21]. Krypton is a colorless inert fluid that is used commercially as a filling gas for energy efficient fluorescent lights [22]. Because of the high flammability of methane and the consequent safety considerations, it was excluded from the study, so krypton and R14 remained as suitable candidates.

1.3. The isothermal Effect, Δh_T

For a Joule Thomson cryocooling, a classic way to maintain a stable working cold temperature is by liquefying a single component coolant, which boiling temperature is pressure dependent only. To attain liquification, the cryocooler's cooling power ($\dot{Q}$) must be greater than the heat load of the Dewar. For a JT cryocooler, the cooling power is a product of the mass flux ($\dot{m}$) and the isothermal effect (Δh_T) [23], (Eq. (1)).

$$\dot{Q} = \dot{m} \bullet \Delta h_T \tag{1}$$

The latter is a difference of enthalpies evaluated at operating pressures and a specific temperature. The operating pressures are defined by the throttling effect, i.e., P_2 and P_6 (Fig. 1). The specific temperature is defined by assuming the cryocooler operates with an ideal heat exchanger, that provides zero temperature difference between the streams' exits (i.e., at point 2 and at point 6, $T_2 = T_6 = T_{amb}$, Fig. 1). The low pressure of an open cycle cryocooler (i.e., P_6) is a fixed value and equals to 0.1 MPa, and the high pressure (i.e., P_2) is a design parameter. The above definition and assumptions lead to the formulation of the isothermal effect, $\Delta h_T = h(0.1MPa, T_{amb}) - h(P_2, T_{amb})$[23], which is a quantity specific to each gas. Therefore Δh_T, is the cooling potential of a gas at specific inlet conditions. The isothermal effect enables to determine the minimum necessary gas consumption required to balance the heat load, a fact that positions the isothermal effect value as an assessing factor for Joule-Thomson cryocoolers' performance [23].

Pressure dependences of the isothermal effect of krypton and R14 at 293 K and 343 K are shown at Fig. 2a and Fig. 2b respectively. The

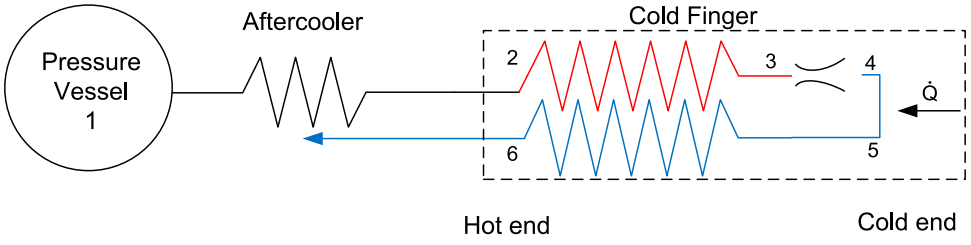

Fig. 1. Open-Cycle JT Cooler General Schematic Drawing.

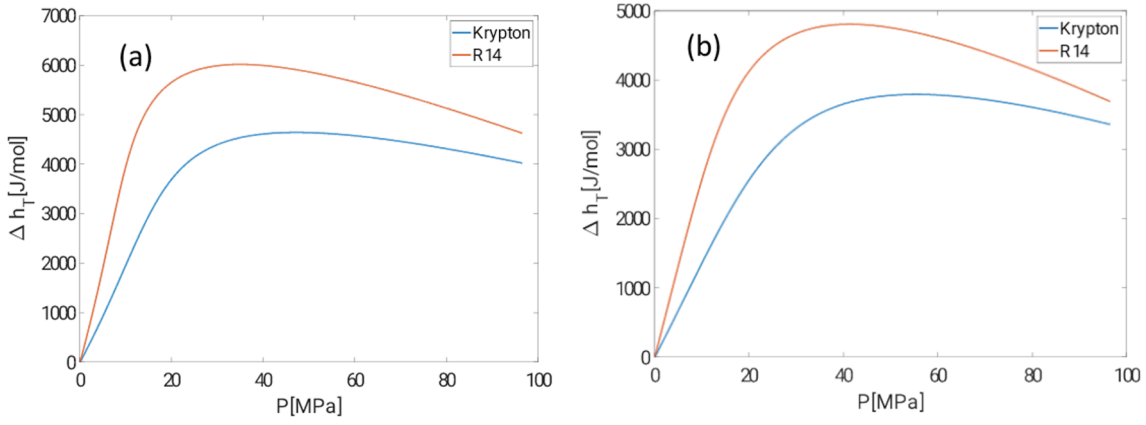

Fig. 2. Comparison between Pressure Dependence of Isothermal Effect of Krypton and R14 at 293 K (a) and at 343 K (b).

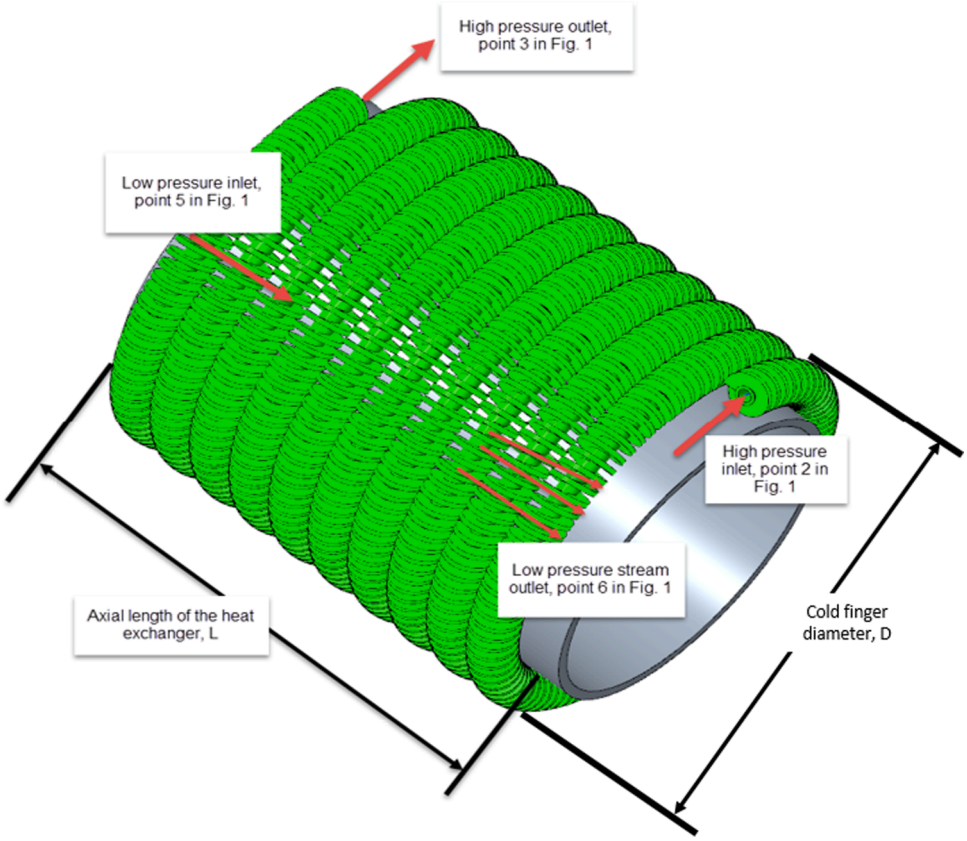

Fig. 3. Schematic View of Finned-Tube JT Heat Exchanger.

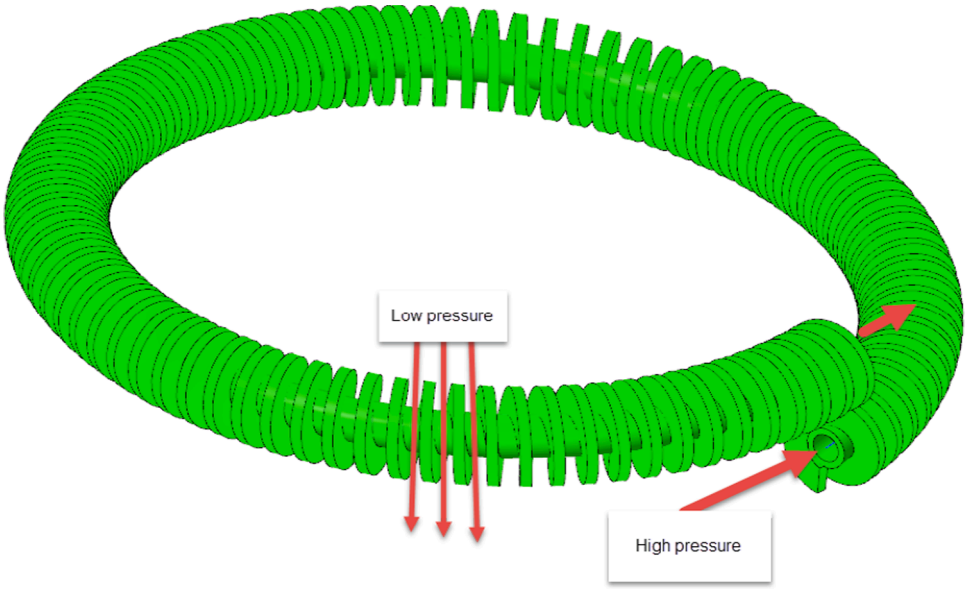

Fig. 4. Single Element of the Simulated Heat Exchanger.

isothermal effect of R14 exceeded krypton's at both temperatures (Δh_T at the peak for R14 was larger by 29.6 % and 26.7 % at 293 K and 343 K respectively). For krypton, maximal values of isothermal effect were obtained at 47.1 MPa (at 293 K) and 55.1 MPa (at 343 K), while for R14 the corresponding values were 34.96 MPa (at 293 K) and 41.52 MPa (at 343 K). Higher values of the isothermal effect of R14, positioned it to show a favorable cooling ability.

1.4. Analysis of a Counter flow Finned-Tube heat exchanger

A schematic view of the heat exchanger is presented at Fig. 3. To investigate heat exchanger properties, the following NTU analysis was implemented [17,18]. The cryocooler's heat exchanger was divided into subsections where each element consists of a single wind of the helical finned tube (see Fig. 4). Due to a counterflow configuration of the cryocooler's heat exchanger for the high-pressure stream (i.e., 'high'

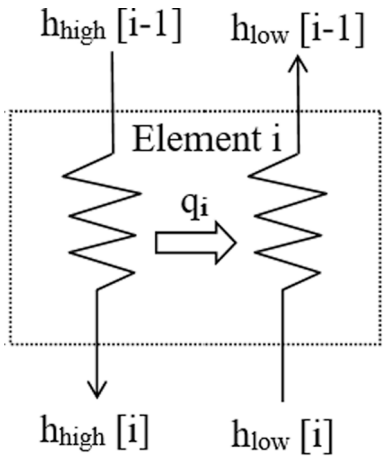

Fig. 5. Schematic View of a Single Element with the Enthalpies' Marking [17].

subscript), the i-th point was the outlet and the i-1 was the inlet, while for the low-pressure stream (i.e., 'low' subscript) the i-th point was the inlet and the i-1 point was the outlet. q_i was the heat transfer rate between the streams (see Fig. 5).

The Outlet enthalpies of each element were calculated according to equations (2) and (3):

$$h_{high}[i] = h_{high}[i-1] - \frac{q_i}{\dot{m}} \tag{2}$$

$$h_{low}[i] = h_{low}[i-1] - \frac{q_i}{\dot{m}} \tag{3}$$

where *i*, was the element index and q_i, was the heat transfer rate between the streams:

$$q_i = \varepsilon_i \bullet C_{min} \bullet \left(T_{high}[i-1] - T_{low}[i]\right) \tag{4}$$

$$C_{min} = \dot{m} \bullet c_{p,min}$$

The heat exchanger effectiveness was calculated using:

$$\varepsilon_i = \frac{1 - e^{(-NTU(1-C_r))}}{1 - C_r \bullet e^{(-NTU(1-C_r))}}, C_r = \frac{C_{min}}{C_{max}} \tag{5}$$

Finally, Number of Transfer Unit (NTU) was defined as the ratio:

$$NTU = \frac{U \bullet A}{C_{min}} \tag{6a}$$

$$U = \frac{1}{\frac{1}{\mathrm{HTC}_{high} \bullet A_{high}} + \frac{ln\left(\frac{d_{t,o}}{d_{t,i}}\right)}{2\pi \bullet k_t \bullet L_t} + \frac{1}{\eta_{fin} \bullet \mathrm{HTC}_{low} \bullet A_{low}}} \bullet \frac{1}{A} \tag{6b}$$

Where *U* was overall heat transfer coefficient, *A* was a heat transfer area, HTC_{high} and HTC_{low} were local convection coefficients of high and low pressure streams respectively, A_{high} and A_{low} were cross-sections of high and low pressure streams respectively, k_t and L_t were conductivity coefficient and thickness of high-pressure stream pipe respectively, and $d_{t,o}$, $d_{t,i}$ were outer and inner diameter of the pipe. η_{fin} was the fin efficiency. Because all properties were calculated locally, a local NTU was obtained, which had varied element-by-element along the heat exchanger.

The thermophysical properties of the fluids (i.e., krypton and R14) were obtained from REFPROP^{TM} software [19]. The correlation of the HTC_{high} was [15,16]:

$$\mathrm{HTC}_{high} = 0.023 \bullet Re^{0.8} \bullet Pr^{\frac{1}{3}} \bullet \left(1 + 3.5\frac{d_{t,i}}{D_H}\right) \bullet \left(\frac{k_{high}}{d_{t,i}}\right) \tag{7}$$

And the correlation for calculating the HTC_{low} was [15]:

Table 2
Heat Exchanger's Dimensions.

Dimension (mm)	Value
Heat exchanger's inner tube diameter	0.27
Heat exchanger's outer tube diameter	0.4
Dewar's inner diameter	11.2
Axial heat exchanger's length	10
Fin's height	0.5
Fin's pitch	0.25
Fin's thickness	0.1

Table 3
Model Validation Results.

P_2 [MPa]	$\dot{m}$[g/s]	T_2 [K]	T_6 [K] acc. to Ng. et.al.	T_6 [K] current simulation	Relative error, Er_r [%]
17.912	0.414	291.49	282.57	281.7	0.3
16.01	0.355	292.25	284.77	283.05	0.6
14.047	0.3	291.94	284.98	281.9	1.08

$$\mathrm{HTC}_{low} = 0.26 \bullet Re^{0.75} \bullet Pr^{\frac{1}{3}} \bullet \left(\frac{k_{low}}{D_{low}}\right) \tag{8}$$

The Reynolds number was defined as follows:

$$Re = \frac{\dot{m} \bullet d}{\mu \bullet A}(\tag{9}$$

Since the experiments were conducted using the same cryocooler for both krypton and R14, the geometric parameters of the heat exchanger assigned in the simulation were the same. Therefore, the differences in cooling performance between krypton and R14 could be attributed to the coolant's heat transfer characteristics.

Geometrical dimensions of the heat exchanger used in the simulation were consistent with the experimental cryocooler's heat exchanger (Figs. 3 and 4 and Table 2).

The main output of the simulation was the minimum axial length of the heat exchanger *L*, which was required to obtain the desired efficiency (Eq. (10)).

$$\eta_{CFHE} = \frac{H(T_6, P_6) - H(T_5, P_5)}{H(T_2, P_6) - H(T_5, P_5)} \tag{10}$$

The heat exchanger model presented here was validated against experimental data obtained by Ng et.al [16]. The experiments were performed with Argon, and to the best of our knowledge there is no data about krypton or R14. The geometric parameters of the heat exchanger and the flow conditions were appropriately adopted to match the experimental setup used by Ng et. al. [16]. The comparison of Ng et al.'s results and the analysis were done by comparing the temperature at the exit of the hot stream (i.e., T_6). The maximal error between Ng et al. [16] results and the reproduced correlation was evaluated according Equation (11) was 1.08% (Table 3).

$$Er_r = \frac{\left((T_6)_{Ng} - (T_6)_{Cur.Sim.}\right)}{(T_6)_{Ng}} \bullet 100\% \tag{11}$$

2. Experimental setup

A 60-cc vessel was filled with the examined coolant and was stabilized at the experimental pressure (i.e., 70 MPa). Its value was measured by a pressure transducer (made by Haenni, Switzerland, accuracy 0.7 % F.S.). The tested assembly consisted of a fixed-orifice JT cryocooler and a matched Dewar. The Dewar had a thermal mass equal to 300 J at temperature of 298 K and its heat load equaled 220 mW for the operational temperature of 120 K (as was specified by the manufacturer). The axial length of the cold finger was 10 mm, and the cold finger diameter was

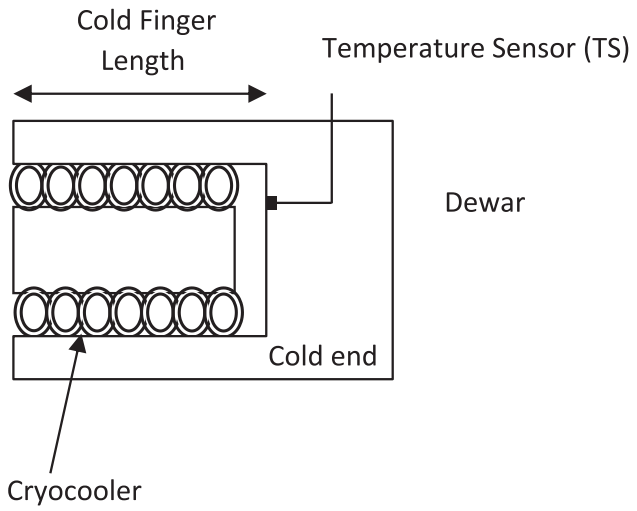

Fig. 6. Schematic View of the Dewar-Cryocooler Assembly.

Table 4
Uncertainty evaluation for the experiments.

	Uncertainty (%)					
	Krypton			R14		
	E_{CDT} (%)	E_{CDP} (%)	E_{CP} (%)	E_{CDT} (%)	E_{CDP} (%)	E_{CP} (%)
293 K	**1.7**	**0.4**	**0.8**	**1.4**	**0.3**	**0.8**
343 K	**1**			**0.7**		

11.2 mm (Fig. 4). The Dewar had a standard double co-axial, vacuumed, cylindric configuration. The Dewar had a PNP transistor 2N2907A, utilized as temperature sensor with accuracy of ± 0.25 K. The sensor was attached to the Dewar's cold end to monitor the cryogenic temperature during the operation (Fig. 6). The flow of the coolant was dependent on the orifice's cross-sectional area, which was 7.85 × 10^{-5} m^2 (the orifice diameter was 0.1 mm and was made by EDM process).

3. Uncertainty analysis

Root mean square analysis [24] was applied for calculating errors for Cool Down Time (CDT), Cooling Duration Period (CDP) and Cutoff Pressure (CP) (Table 4). The accounted parameters for the errors were: pressure transducer's offset point, cold end's temperature sensor calibration accuracy, accuracy of the environmental chamber's temperature (i.e., T_{amb}). The uncertainties were presented as a percentage of the readings and summarized in Table 4. Additionally, the mass flow rate was calculated based on the vessel pressure and the ambient temperature (Eq. (12)). Therefore, integrating the two mentioned quantities led to an uncertainty of 10 % in the mass flow rate for krypton and 12.5 % for R14.

3.1. Experimental procedure

The Dewar-cryocooler assembly was placed in an environmental chamber and connected to a pressure vessel that was filled with the investigated coolants (i.e., krypton or R14) (Fig. 7). After the pressure vessel was filled, a 30-minute period was timed to enable the pressure vessel to reach thermal equilibrium with the environment. Then, chamber's temperature was set to the testing temperature (i.e., 293 K or 343 K), and another 120 min were timed for the system to reach the temperature and to stabilize thermally.

The measured parameters (i.e., cold end's temperature and the vessel's pressure) were recorded using data translation DT 9806 data acquisition module (DAQ) with sampling rate of 20 Hz.

At the beginning of the experiment the data recording was commenced, and the vessel valve was opened to allow the coolant to flow through the cryocooler. The recording was halted when the cold end's temperature increased at least by 8 K compared to the cold steady temperature.

4. Results and discussion

4.1. Experimental results

The Cool Down Time (CDT) was defined as the time required the cold end's temperature to drop to a 3 K margin from the steady state value. The Cooling Duration Period (CDP) was defined as the time that the temperature was maintained within a 3 K margin from the steady state value, and the Cutoff Pressure (CP) was defined as the vessel pressure value at which the cooling process ended. These parameters characterize cooling performance. Because the cooling process depended on the vessel discharging rate (i.e., instantaneous flow rate of the cryocooler), the total cooling time was limited by amount the gas in the vessel. Thus,

Table 5
Experimental results summary.

	Krypton			R14		
	CDT (sec)	CDP (sec)	CP (MPa)	CDT (sec)	CDP (sec)	CP (MPa)
293 K	**3**	**160**	**0.93**	**3.8**	**146**	**1.77**
343 K	**5.6**	**147**	**1.32**	**7.6**	**120**	**5.1**

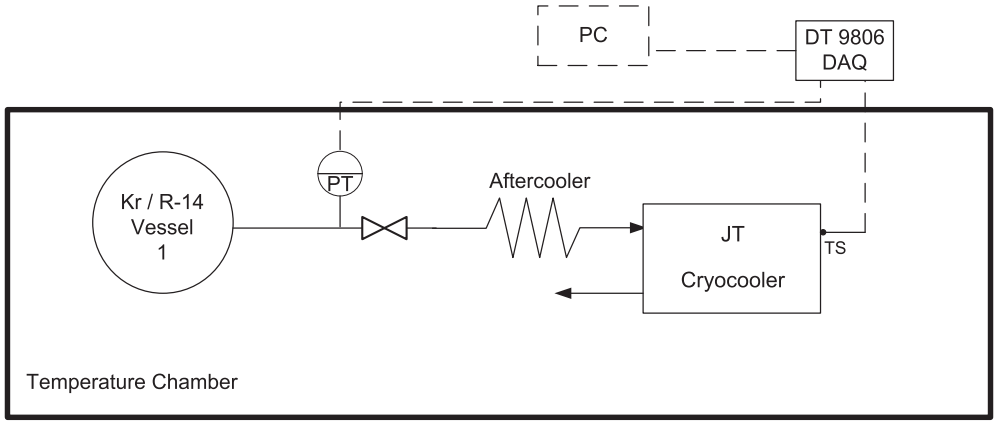

Fig. 7. Experimental Setup (continuous lines indicate pneumatic pipes; dashed lines indicate electric cables).

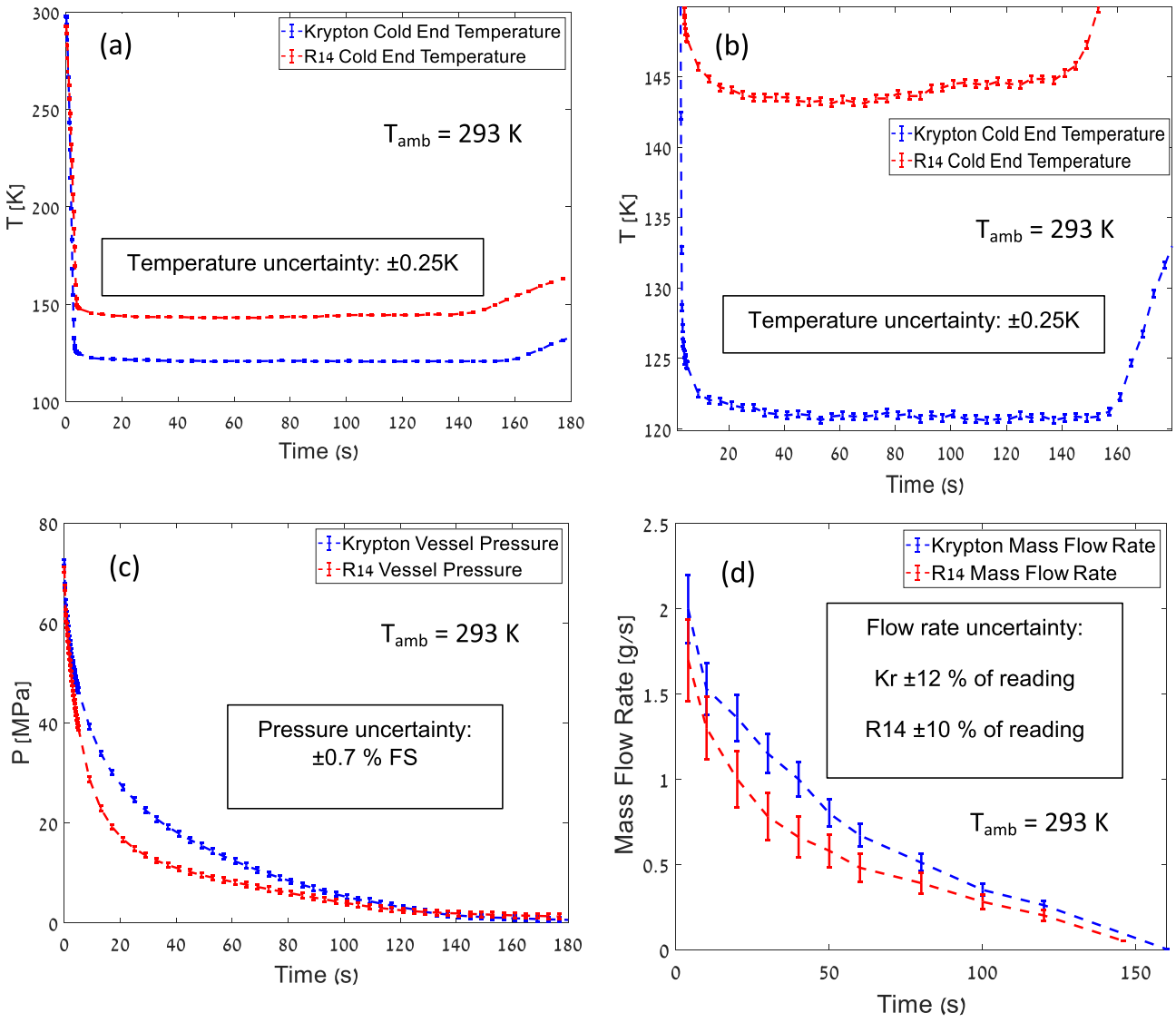

Fig. 8. Krypton and R14 Experimental Data at 293 K Ambient Temperature, a – Cold End Temperature Full Process, b – Cold End Temperature Zoom into Steady Region, c- Vessel Pressure, and d- Mass Flow Rate.

CDP was the time that the cryocooler maintained steady boiling temperature. CP was indicative to the heat exchanger performances and helped to examine CDP, Table 5.

The cold end's temperatures (Figs. 8a-b and 9a-b) and vessel pressure (Fig. 8c and Fig. 9c) were monitored during the experiments for ambient temperature of 293 K and 343 K. The mass flow rates (Fig. 8d, and Fig. 9d) were calculated from the pressure profile using Eq. (12).

$$\dot{m} = \dot{\rho}\left(\dot{P}\right) \bullet V \tag{12}$$

where $\dot{m}$ is the mass flow rate, $\dot{\rho}$ is the pressure dependent density gradient and the V is the vessel volume.

Since the vessel was filed at 293 K for both experiments the initial mass of the coolant was similar for both ambient temperatures. However, the initial pressure was different for 293 K and 343 K. The pressures were 75 MPa for 293 K and 95 MPa for 343 K (Fig. 8c and Fig. 9c). The charged masses for krypton and R14 were 106.75 gr and 78.96 gr, respectively. In both cases, the pressure profiles declined with decreasing rate, these profiles were characteristic to vessel discharge processes. The mass flow rates of the cryocooler were proportional to the pressure and therefore, had a similar trend (Fig. 8c and Fig. 9c). The initial mass flow rates for krypton were 1.9 gr/s and 2.4 gr/s for 293 K and 343 K, respectively, and for R14 1.8 gr/s and 1.6 gr/s, respectively. For krypton, higher mass flux for higher ambient temperature was a result of higher pressure inside the vessel, which led to earlier discharge time because the initial total masses of the coolants were the same. For both ambient temperatures, R14 discharged earlier than krypton due to higher compressibility of the fluid.

In both cases, the cold end's temperature decreased rapidly until reaching boiling temperatures (i.e., about 120 K and about 145 K for krypton and R14, respectively). The timing from the opening of the valve to 3 K above the boiling temperature (i.e., CDT) at ambient temperature of 293 K, were 3 s and 3.8 s, for krypton and R14, respectively. The CDTs at ambient temperature of 343 K were 5.6 K and 7.6 K for krypton and R14, respectively (see Table 4). Following the cooldown, the existence of a liquid phase inside the Dewar fixed the measured temperature, which stabilized the temperature readings in both cases. The CDPs for 293 K experiments were 160 s and 146 s for krypton and R14, respectively, and the CDPs for 343 K experiments were 147 s and 120 s for krypton and R14, respectively. For higher ambient temperatures, the Dewar's heat load was larger, which shortened the CDPs (Table 5). Towards the end of the cooling, the cryocooler ceased to produce liquid due to low inlet pressure. The produced liquid boiled away due to Dewar's thermal load, and the cold end's temperature

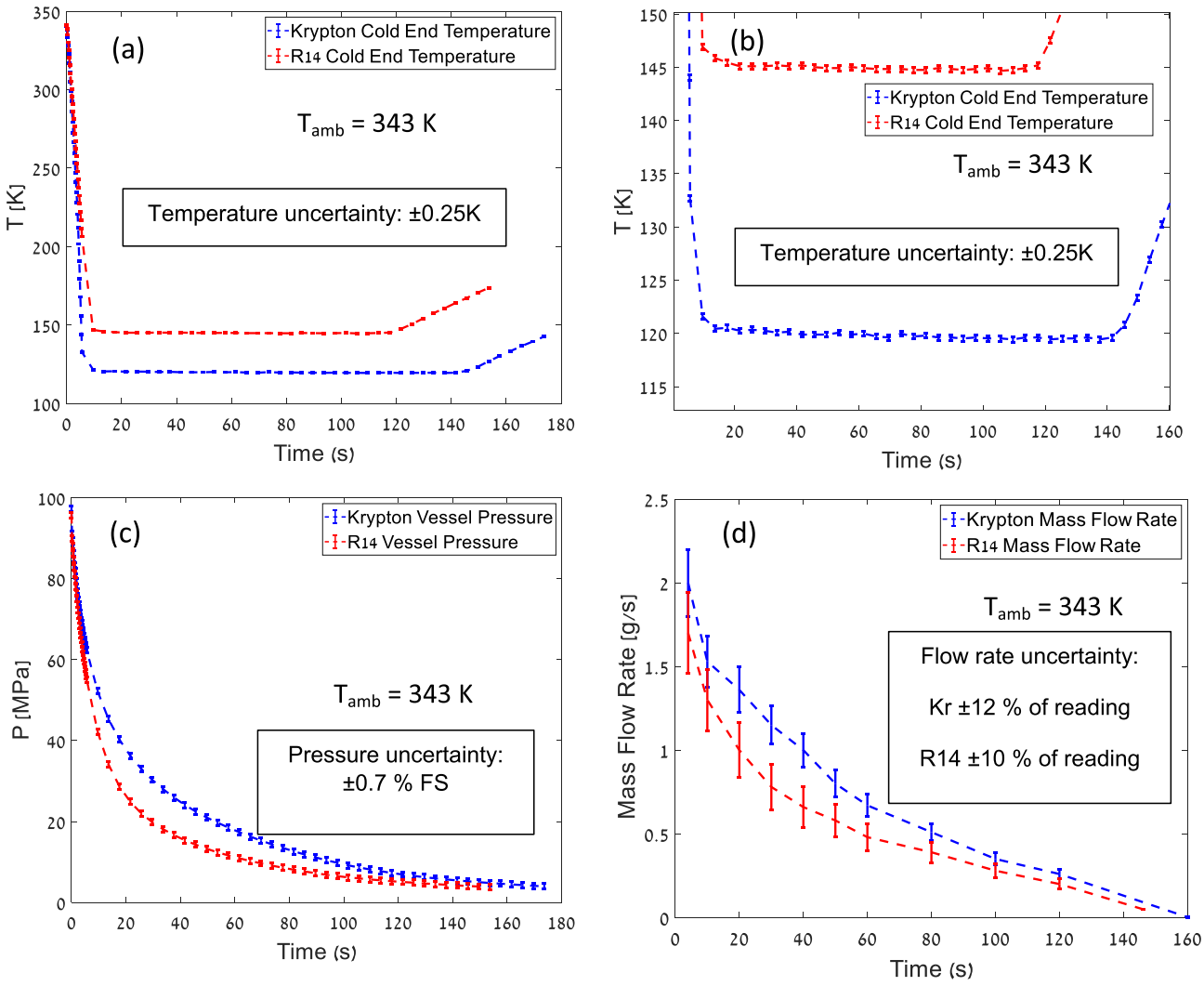

Fig. 9. Krypton and R14 Experimental Data at 343 K Ambient Temperature, a – Cold End Temperature Full Process, b – Cold End Temperature Zoom into Steady Region, c- Vessel Pressure, and d- Mass Flow Rate.

started to rise. When the measured temperature rose 3 K above the boiling temperature (i.e., about 123 K and about 148 K for krypton and R14, respectively) the CP was gauged. The CPs for 293 K experiment were 0.93 MPa and 1.77 MPa and for the 343 K experiment were 1.32 MPa and 5.1 MPa for krypton and R14, respectively. The higher values were indicative of a higher thermal load at ambient temperature of 343 K. In the described experimental setting and for the examined ambient temperatures, krypton outperformed R14 in all the examined parameters (i.e., CDT, CDP, and CP).

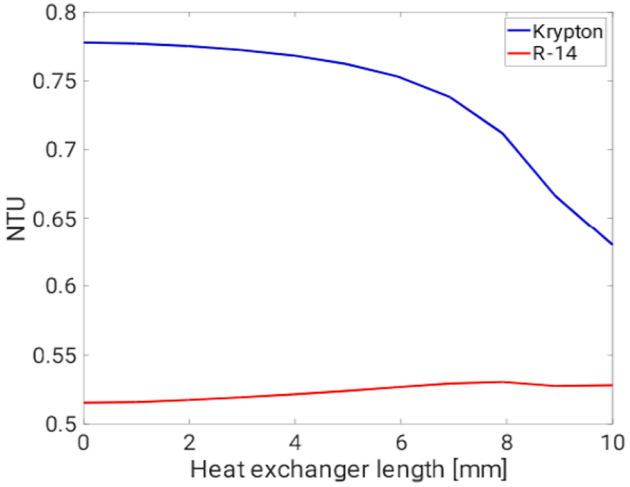

Fig. 10. Comparison between NTU for Both Coolants, Produced Using Equations (5) and (6).

4.2. *Theoretical comparison of the coolants at the tested conditions*

The isothermal effect was proportional to the inlet pressure for values less than 30 MPa and 35 MPa for R14 and krypton, respectively, and inversely proportional for higher pressures (Fig. 2). In addition, for fixed orifice (as realized in the current cryocooler) the flow rate was proportional to the inlet pressure. Effective cooling power of a cryocooler, measured in Watts, was defined as the product of the isothermal effect, heat exchanger's efficiency and the mass flow rate (Equation (13)). For both krypton and R14, the change in mass flow rate due to increase in the pressure overshadows the decrease in the isothermal effect of the coolants, and, therefore, the cooling power increased as the pressure increased.

$$\dot{Q}_{eff} = \Delta h_T \bullet \dot{m} \bullet \eta \tag{13}$$

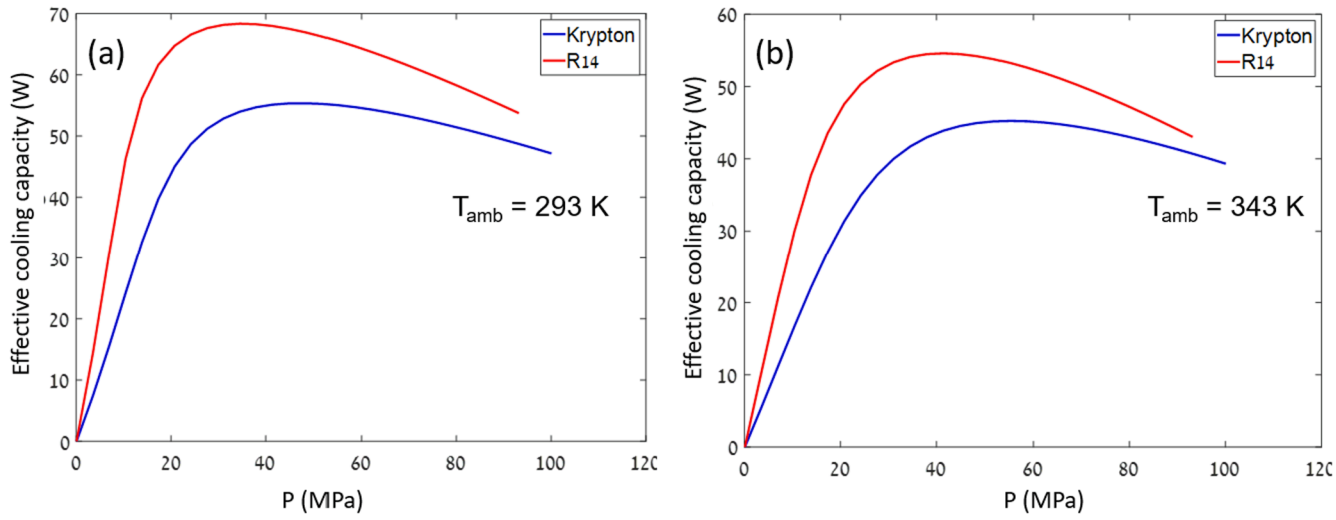

Fig. 11. Effective cooling capacity for krypton and R14, at 293 K (a) and at 343 K (b).

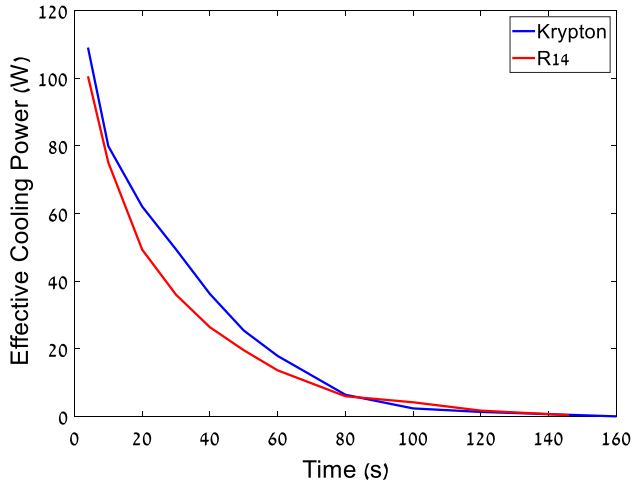

Fig. 12. Calculation of the Effective Cooling Power for Both Coolants at 293 K Temperature Tests.

4.3. Cryocooler's heat exchanger performance

The examined cryocooler had a 10 mm long heat exchanger (see Figs. 3 and 4 and Table 2). By applying NTU analysis described in section 'Analysis of a Counter Flow Finned-Tube Heat Exchanger', heat exchanger's efficiencies. for krypton and R14 were equaled to 0.94 and 0.85, respectively.

The NTU of both coolants was calculated under constant inlet conditions, i.e., inlet pressure and flow rate were constant, which was different from the experimental conditions. Since the cryocooler was a non-regulated and therefore, the pressure and the mass flow were time dependent. To account for this difference, median values of the experiments were used as inputs for the analysis calculations. The inlet high pressure (i.e. P_2) and the flow rate were set to 40 MPa and 1 g/sec respectively.

The NTU was calculated for each revolution of the heat exchanger where x = 0 was the hot end and x = 10 mm was the cold end of the heat exchanger (Fig. 10). The NTU of krypton at the hot end (i.e., x = 0 mm) had the largest value and equaled to about 0.77, as the revolution distanced from the hot end the NTUs reduced to about 0.63 at the cold end. R14′s NTU trend was opposite to krypton (i.e., the NTU increased as coolant's temperature dropped). At the hot end (i.e., x = 0 mm) the NTU was minimal and equaled about 0.51 and at the cold end (i.e., x = 10 mm) the NTU reached 0.525. However, for the examined heat exchanger, krypton's NTU was higher than R14′s NTU though the entire length. According to Equation (5), higher NTU increased the heat exchanger effectiveness and thus increased the heat exchanger efficiency.

Effective cooling capacity, measured in Watts, was defined by Eq. (13) where the mass flow rate was set to 1 gr/s (i.e., effective cooling capacity equals $\Delta h_T \bullet \eta$). Dependence of the effective cooling capacity to the high pressure for both coolants was shown in Fig. 11a at 293 K ambient temperature and Fig. 11b at 343 K ambient temperature. This term isolated the role of isothermal effect in heat exchanger's performances assuming similar flow rate. Since heat exchanger's efficiencies were relatively constant the effective cooling capacity had a trend like that of the isothermal effect (Fig. 2). The maximal values of R14′s effective cooling capacity exceeded krypton's by about 15 W depending on the ambient temperature. The difference in the maximal values decreased with the increase of the ambient temperature. Finally, the effective cooling capacity of R14 was higher than of krypton for the measured pressure range (from 0 MPa to about 100 MPa).

Fig. 12 shows the calculation of the effective cooling power during the test at 293 K ambient temperature, for both coolants. During the first 80 s, krypton overperformed R14, by providing significantly larger effective cooling power. Since at ambient temperature of 293 K the Dewar required only 0.22 W to maintain the temperature difference, the excessive effective cooling power was translated into liquid phase accumulation inside Dewar's evaporator (i.e., at the cold end). Initially, both coolants provided excessive effective cooling power and generated a volume of liquid at the cold end of the Dewar. The accumulated liquid functioned as a heat sink through the vessel's discharge, and the coolants' accumulation significantly prolonged the CDP [25]. Providing excessive amount of effective cooling power has its pros and cons, the positive effect was the reduction in CDP, since the Dewar was overwhelmed by cold coolant, which accelerated the cooldown process. On the other hand, high flow rate could discharge liquid coolant out of the Dewar and by doing so to reduce the CDP of the Dewar.

Finally, to characterize and compare the performance of JT cryocooler, all three terms (i.e., coolant's isothermal effect, heat exchanger's efficiency, and mass flow rate) of the effective cooling power needed to be evaluated. Despite higher isothermal effect of R14, krypton demonstrated better CDT and CDP. That can be explained by higher effective cooling power caused by higher mass flow rate in the examined configuration of the cryocooler.

For an unregulated cryocooler (i.e., where the mass flow rate is a function of the inlet pressure), the mass flow rate turned out to be the

most important parameter for cooling performances. On the other hand, for a regulated cryocooler where the flow rate is a function of Dewar's heat load, no liquid should be accumulated at the cold end, the coolant's effective cooling capacity should be the dominant factor to evaluate cryocooler performance and therefore, R14 should perform better than krypton.

5. Summary and conclusions

The objective of this study was to identify single component coolants for working temperatures between 100 K and 150 K and consequently to test coolants' performances using unregulated JT cryocooler. Following sorting of boiling and the freezing temperatures, krypton and R14 were identified as potential coolants and consequently tested. For the examined cryocooler, krypton overperformed R14 in CDT, CDP, and CP. Within the framework of theoretical analysis of the heat exchanger efficiency, all the discrete parameters like Reynolds numbers, viscosity, and overall heat transfer coefficient have provided inconclusive results. The better performance of krypton was further explained in terms of the isothermal effect, effective cooling capacity, and effective cooling power. For unregulated cryocooler, mass flow rate was found to be the most influential parameter on the effective cooling power and, therefore, the most influential parameter on system performance.

CRediT authorship contribution statement

Alexander Shapiro: Conceptualization, Methodology, Software, Validation, Formal analysis, Investigation, Writing – original draft, Supervision. **Mordechai Greenberg:** Resources, Visualization. **Anatoly Parahovnik:** Investigation, Data curation, Writing – review & editing.

Declaration of Competing Interest

The authors declare that they have no known competing financial interests or personal relationships that could have appeared to influence the work reported in this paper.

References

[1] Radebaugh R. Pulse tube cryocoolers. Low Temperatures and Cryogenic Refrigeration 2003:415–34.

[2] Adams A., Advances in Detectors: HOT IR Sensors Improve IR Camera Size, Weight, and Power, https://ircameras.com/articles/advances-detectors-hot-ir-sensors-improve-ir-camera-size-weight-power/.

[3] Radebaugh R, Bradley P, Coolidge C, Lewis R, Lee YC. "Design and Analysis of a 150 K Cascade Joule-Thomson Microcooler", Cryocoolers 18 International Cryocooler Conference Inc. CO: Boulder; 2014.

[4] Piotrowska A, Chorowski M, Dorosz P. Performance Analysis of Joule-Thomson Cooler Supplied with Gas Mixtures. IOP Conf Series: Materials Science and Engineering 2017;171.

[5] Tzabar N. Binary mixed-refrigerants for steady cooling temperatures between 80 K and 150 K with Joule Thomson cryocoolers. Cryogenics 2014;64:70–6.

[6] Walimbe NS, Narayankhedkar KG, Atrey MD. Experimental Investigation on Mixed Refrigerant Joule Thomson Cryocooler with Flammable and Non-Flammable Refrigerant Mixtures. Cryogenics 2010;50:653–9.

[7] Xu M, He Y, Chen Z. Analysis of Using Binary Cryogenic Mixtures Containing Nitrogen and Alkanes or Alkenes in Cryocoolers. Cryogenics 1996;36:69–73.

[8] Xu M, He Y, Chen Z. Analysis of Binary Cryogenic Mixtures Containing Nitrogen and Freon in Cryocoolers. Cryogenics 1996;36:243–7.

[9] Geng H, Cui X, Weng J, She H, Wang W. Review of Experimental Research on Joule-Thomson Cryogenic Refrigeration System. Appl Therm Eng 2019;157:113640.

[10] Shapiro A., Fraiman L., Parahovnik A., " Ceramic 3D Printed Joule Thomson Mini Cryocooler Intended for HOT IR Detectors", Proc SPIE (2017) 10180.

[11] Ardhapurkar PM, Atrey MD. Performance Optimization of a Miniature Joule-Thomson Cryocooler Using Numerical Model. Cryogenics 2014;63:94–101.

[12] Damle RM, Atrey MD. Transient Simulation of a Miniature Joule-Thomson (J–T) Cryocooler with and without the Distributed J-T Effect. Cryogenics 2015;65:49–58.

[13] Gupta PK, Kush PK, Tiwari A. Experimental Research on Heat Transfer Coefficients for Cryogenic Cross-Counter-Flow Coiled Finned-Tube Heat Exchangers. Int J Refrig 2009;32(5):960–72.

[14] Gupta PK, Kush PK, Tiwari A. Experimental Studies on Pressure Drop Characteristics of Cryogenic Cross-Counter Flow Coiled Finned Tube Heat Exchangers. Cryogenics 2010;50(4):257–65.

[15] Mehta, S. M., Damle, R. M., Desai, K. P., and Naik, H. B., 2019, "Theoretical and Experimental Study of Coiled Finned Tube Heat Exchanger for Helium Liquefaction Plant," *IOP Conference Series: Materials Science and Engineering*, IOP Publishing, p. 012016.

[16] Ng KC, Xue H, Wang JB. Experimental and Numerical Study on a Miniature Joule-Thomson Cooler for Steady-State Characteristics. Int J Heat Mass Transf 2002;45(3):609–18.

[17] Tzabar N., "A Numerical Study on Recuperative Finned-Tube Heat Exchangers", Cryocoolers 18.

[18] Hong Y-J, Park S-J, Choi Y-D. A numerical study of the performance of a heat exchanger for a miniature Joule-Thomson refrigerator. Cryocooler 2009;15:379–86.

[19] Lemmon, E.W., Bell, I.H., Huber, M.L., McLinden, M.O. NIST Standard Reference Database 23: Reference Fluid Thermodynamic and Transport Properties-REFPROP, Version 10.0, National Institute of Standards and Technology, Standard Reference Data Program, Gaithersburg, 2018.

[20] Mauer JL, Logan JS, Zielinski LB, Schwartz GC. Mechanism of Silicon Etching by a CF4. Journal of Vacuum Science and Technology 1978;15:1734.

[21] Thunnissen DP, Guernsey CS, Baker RS, Miyake RN. Advanced Space Storable Propellants for Outer Planet Exploration. AIAA 2004–3488..

[22] https://www.rsc.org/periodic-table/element/36/krypton.

[23] B-Z. Maytal, J. M. Pfotenhauer, "Miniature Joule-Thomson Cryocooling: Principles and Practice", Springer Science & Business Media (2012).

[24] Moffat RJ. Describing the Uncertanies in Experimental Results. Exp Therm Fluid Sci 1988.

[25] Tzabar N, Lifshiz I, Kaplansky A. Fast Cool-Down J-T Cryocooler to 88K. Adv Cryog Eng 2008;53.